Euro. Jnl of Applied Mathematics (2013), *vol.* 24, *pp.* 77–101.
doi:10.1017/S0956792512000319

Topology of two-dimensional flow associated with degenerate dividing streamline on a free surface

A. DELİCEOĞLU

Department of Mathematics, Erciyes University, Kayseri 38039, Turkey
email: adelice@erciyes.edu.tr

(*Received 2 January 2012; revised 1 September 2012; accepted 3 September 2012; first published online 25 September 2012*)

Topology of two-dimensional flow associated with degenerate dividing streamline on a free surface is analysed from a topological point of view by considering the critical point concept. Streamline patterns and their bifurcations in the vicinity of a free surface were investigated by Brøns (Brøns, M. (1994) Topological fluid dynamics of interfacial flows. *Phys. Fluids* **6**, 2730–2736). Brøns's work is extended to the case of a stream function, including the fourth-order normal form approach. From this, a complete description of bifurcations which can occur in two-dimensional incompressible flow is obtained up to codimension three. The theory is applied to the patterns found numerically in a roll coater.

Key words: Dynamical systems in fluid mechanics (37N10); Incompressible viscous fluids (76D99); Bifurcation problems

1 Introduction

The topological fluid dynamics of flows with interfaces and free surfaces is a topic of interest, with a wide variety of scientific and engineering applications (see [3, 10, 14, 17, 20, 21]).

There has been a great deal of work on nonlinear dynamics. Important studies on this topic appeared in the early 1980s (for example [15, 16, 18]). An elementary property of stable singularities is discussed by Golubitsky and Guillemin [9]. An investigation of local flow properties on a viscous free surface has been conducted through nonlinear dynamics; this approach provides a coherent theoretical framework and deduces flow patterns based on the saddles and centres, and the lines of separation and attachment on a viscous-free surface. Nonlinear dynamics was first applied to flows near fluid interfaces by Lugt [14]. He studied dividing streamlines, curvature effects and the role of vorticity, and derived some basic properties of flow on a viscous-free surface; for example a single dividing streamline is always perpendicular to the free surface. Lugt's [14] work was revisited in a more general setting, allowing the interface to take an arbitrary shape by Brøns [3]; he discovered a complete description of the bifurcations that depend on terms of up to the second order.

In this study, a normal form transformation is used for constructing a simple stream function family, which classifies all possible local streamline topologies for a given order of degeneracy (degeneracy of order 4 is considered). This technique was first used by

Brøns and Hartnack [5] for two-dimensional (2D) flow away from boundaries, and by Hartnack [13] for 2D flow close to fixed (possibly curved) walls. This approach was later used to analyse a variety of specific steady flows, for example the flow in a driven cavity [8, 11], slip flows [19], a flow close to an axisymmetric flow [2] and vortex breakdown [4, 7].

In the present work, the streamline topology of a 2D incompressible flow near the critical point is studied. Critical points are degenerate in the sense that the Jacobian of linearisation of the corresponding Hamiltonian dynamical system about such a critical point vanishes identically. There are two types of degenerate critical points (simple and non-simple degeneracies) which depend on the Jacobian matrix of the velocity field. The first case, concerning simple degenerate critical points (i.e. a singular yet non-zero Jacobian matrix), was examined by Hartnack [13]. The second case, concerning non-simple degenerate critical points (i.e. vanishing Jacobian), was examined theoretically and numerically by Gürcan *et al.* [12], who discovered streamline patterns and their bifurcations near a non-simple degenerate critical point. The unfolding of degenerate patterns, which means a family of stream functions containing a particular degenerate flow, may be obtained up to codimension three. These degenerate patterns are classified by their codimension, which is the number of their unfolding parameters. For codimension three, corresponding to the fourth-order normal form of the stream function, we obtain a flow pattern with three critical points on a free surface connected with an in-flow saddle point to produce two separation bubbles with opposite rotations. In the case of flows near a wall, such a pattern was predicted in the theoretical works of Bakker [1] and Gürcan *et al.* [12]. The same structure was realised in the near-wake of a circular cylinder at low Reynolds numbers by Brøns *et al.* [6].

The aim of this paper is to find the streamline patterns and their bifurcations in a 2D incompressible fluid flow near a non-simple degenerate critical point close to a free surface. A normal form transformation is used to simplify the differential equations of a Hamiltonian system that describes the streamlines. It will be shown that degenerate flow patterns and their bifurcations associated with the non-simple degenerate critical point near a stationary wall can also be seen near a free surface under certain conditions. The theory is applied to the pattern found numerically in the studies of Stokes flow in a roll coater. Also, a new degenerate critical point is found on the free surface. Their bifurcations give rise to a variety of flow patterns which have not been observed previously either theoretically or numerically.

2 Governing differential equations and boundary condition of 2D motion

The steady, isothermal flow of an incompressible, Newtonian fluid of uniform density, ρ, and viscosity, μ, is given by the Navier–Stokes equation

$$\rho \mathbf{u} \nabla \mathbf{u} = -\nabla \mathbf{p} + \mu \nabla^2 \mathbf{u} + \rho \mathbf{g} \tag{2.1}$$

expressing the conservation of momentum, and the continuity equation

$$\nabla \cdot \mathbf{u} = 0 \tag{2.2}$$

https://doi.org/10.1017/S0956792512000319 Published online by Cambridge University Press

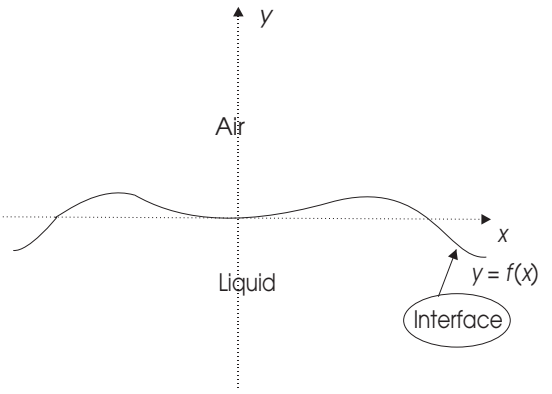

FIGURE 1. The geometry of the problem. The interface is given by the curve $y = f(x)$ with liquid below and air above.

embodying the conservation of fluid mass. Here $\mathbf{u} = (u, v)$ and $\mathbf{p}$ are the fluid velocity and pressure, respectively, and $\mathbf{g}$ is the acceleration due to gravity. We consider the steady, 2D flow of a liquid–gas interface or a free surface. The interface is given by $y = f(x)$ with liquid below and gas above. We assume that the coordinate system is translated and rotated such that $f(0) = f'(0) = 0$ (see Figure 1).

The presence of moving fluid–fluid interfaces introduces complications into the solution procedure, since the shapes of these boundaries are not known *a priori* and must be determined as a part of the solution. Thus, this interface in a 2D flow is a curve of unknown shape that may be fitted locally by a polynomial about the origin. Assuming that the interface is smooth, we can write

$$f(x) = \sum_{n=2}^{\infty} s_n x^n. \tag{2.3}$$

A stream function ψ results from the continuity equation such that the streamlines are found from

$$\dot{x} = u = \frac{\partial \psi}{\partial y}\,, \qquad \dot{y} = v = -\frac{\partial \psi}{\partial x}\,. \tag{2.4}$$

To obtain local information about the flow close to a given point that is taken as the origin, ψ, is expanded in a Taylor series,

$$\psi = \sum_{i+j=0}^{\infty} a_{i,j} x^i y^j. \tag{2.5}$$

Here we consider the coefficients of the series at some finite order, so the analyticity of ψ is not important.

On the free surface (a) the normal velocity must vanish, (b) the tangential (shear) stress must be continuous and (c) the normal stresses and surface tension stresses must balance.

https://doi.org/10.1017/S0956792512000319 Published online by Cambridge University Press

The first condition, written as $\mathbf{u}\cdot\mathbf{n}=0$ (in terms of the stream function)

$$-f'(x)\frac{\partial\psi}{\partial y}=\frac{\partial\psi}{\partial x}, \tag{2.6}$$

is known as the kinematic boundary condition and expresses the fact that no fluid may cross a steady interface. Here $\mathbf{u}$ is the velocity vector and $\mathbf{n}=(1+f'(x)^2)^{-1/2}(-f'(x),1)$ is the normal vector of the interface at $(x,f(x))$.

Inserting the expansions (2.3) and (2.5) into (2.6) yields

$$\begin{aligned} a_{1,0} &= 0, \quad a_{2,0}=-s_2a_{0,1}, \quad a_{3,0}=-s_2a_{1,1}-s_3a_{0,1}, \\ a_{4,0} &= -s_3a_{1,1}-a_{2,1}s_2-a_{0,2}{s_2}^2-s_4a_{0,1} \end{aligned} \tag{2.7}$$

and the stream function (2.5) becomes

$$\begin{aligned} \psi &= a_{0,1}y-s_2a_{0,1}x^2+a_{1,1}xy+a_{0,2}y^2+(-s_2a_{1,1}-s_3a_{0,1})x^3 \\ &\quad +a_{2,1}x^2y+a_{1,2}xy^2+a_{0,3}y^3+(-s_3a_{1,1}-a_{2,1}s_2-a_{0,2}{s_2}^2-s_4a_{0,1})x^4 \\ &\quad +a_{3,1}x^3y+a_{2,2}x^2y^2+a_{1,3}xy^3+a_{0,4}y^4. \end{aligned} \tag{2.8}$$

When one of the fluids is air and the other is liquid, as in this paper, the fact that the viscosity of air is negligible compared to that of most liquids means that condition (b) is reduced to

$$(\mathbf{n}\cdot\sigma)\cdot\mathbf{t}=\mathbf{0}, \tag{2.9}$$

where $\sigma=-pI+[\nabla\mathbf{u}+(\nabla\mathbf{u}^T]$ is the stress tensor of the liquid, $\mathbf{n}$ is the unit normal pointing outwards from the liquid and $\mathbf{t}$ is the unit tangent to the free surface. The boundary condition (2.9) can be expressed in terms of the stream function as

$$-4\mu f'(x)\left(\frac{\partial^2\psi}{\partial x\partial y}\right)+\mu\left(\frac{\partial^2\psi}{\partial y^2}-\frac{\partial^2\psi}{\partial x^2}\right)(1-f'(x)^2)=0, \tag{2.10}$$

and inserting the expansions (2.3) and (2.8) into (2.10) gives a sequence of relations between the Taylor coefficients a_{ij}. The first few are

$$\begin{aligned} a_{0,2} &= -s_2a_{0,1}, \quad a_{1,2}=s_2a_{1,1}-3\,s_3a_{0,1}, \\ a_{2,2} &= 3\,a_{2,1}s_2-6\,s_4a_{0,1}-3\,a_{0,3}s_2+6\,{s_2}^3a_{0,1}. \end{aligned} \tag{2.11}$$

So the stream function becomes

$$\begin{aligned} \psi &= a_{0,1}y-s_2a_{0,1}x^2+a_{1,1}xy-s_2a_{0,1}y^2+(-s_2a_{1,1}-s_3a_{0,1})x^3 \\ &\quad +a_{2,1}x^2y+(s_2a_{1,1}-3\,s_3a_{0,1})xy^2+a_{0,3}y^3+(-s_3a_{1,1}-a_{2,1}s_2 \\ &\quad +{s_2}^3a_{0,1}-s_4a_{0,1})x^4+a_{3,1}x^3y+(3\,a_{2,1}s_2-6\,s_4a_{0,1}-3\,a_{0,3}s_2+6\,{s_2}^3a_{0,1})x^2y^2 \\ &\quad +a_{1,3}xy^3+a_{0,4}y^4. \end{aligned} \tag{2.12}$$

The last boundary condition (c) applied at the free surface is the normal stress condition

$$(\mathbf{n}\cdot\sigma)\cdot\mathbf{n}=\frac{T}{R}, \tag{2.13}$$

https://doi.org/10.1017/S0956792512000319 Published online by Cambridge University Press

where $R = \frac{(1+f'(x)^2)^{3/2}}{f''(x)}$ is the radius of the curvature of the interface at $(x, f(x))$ and T is the surface tension, which is assumed to be constant over the entire free surface. Equation (2.13) can be written in terms of the stream function as follows:

$$-p(x,y)(1+f'(x)^2) + 2\mu f'(x)^2 \frac{\partial^2}{\partial x \partial y}\psi(x,y) - 2\mu \frac{\partial^2}{\partial x \partial y}\psi(x,y) \tag{2.14}$$
$$-2\mu f'(x)\left(\frac{\partial^2}{\partial y^2}\psi(x,y) - \frac{\partial^2}{\partial x^2}\psi(x,y)\right) = \frac{f''(x)T}{\sqrt{1+f'(x)^2}}.$$

For equation (2.14), the pressure coefficients must be determined. It can be expanded in a series

$$p(x,y) = \sum_{i+j=0}^{\infty} p_{i,j} x^i y^j. \tag{2.15}$$

By applying the Navier–Stokes equation (2.1), we obtain the pressure series as follows:

$$\begin{aligned} p(x,y) = {} & p_{0,0} + (-\rho a_{0,1}a_{1,1} + 2\mu a_{2,1} + 6\mu a_{0,3})x + (-2\rho {a_{0,1}}^2 s_2 + 4\mu s_2 a_{1,1} \\ & + 12\mu s_3 a_{0,1})y + (-\rho a_{0,1}a_{2,1} + 2\rho {s_2}^2 {a_{0,1}}^2 - \frac{\rho {a_{1,1}}^2}{2} + 3\mu a_{3,1} \\ & + 3\mu a_{1,3})x^2 + (-6\rho a_{0,1}s_2 a_{1,1} - 6\rho {a_{0,1}}^2 s_3 + 24\mu s_3 a_{1,1} + 12\mu a_{2,1}s_2 \\ & - 48\mu {s_2}^3 a_{0,1} + 48\mu s_4 a_{0,1} + 12\mu a_{0,3}s_2)xy + (\rho a_{0,1}a_{2,1} + 2\rho {s_2}^2 {a_{0,1}}^2 \\ & - \frac{\rho {a_{1,1}}^2}{2} - 3\mu a_{3,1} - 3\mu a_{1,3})y^2. \end{aligned} \tag{2.16}$$

Inserting equations (2.12) and (2.16) into equation (2.14) yields

$$a_{1,1} = \frac{-p_{0,0} + 2s_2 T}{2\mu}, a_{2,1} = -\frac{p_{0,0}\rho a_{0,1} - 2\rho a_{0,1}s_2 T + 12\mu^2 a_{0,3} - 12 s_3 T\mu}{12\mu^2}, \tag{2.17}$$

$$a_{3,1} = \frac{-16\mu {s_2}^2 a_{1,1} - 24 {s_2}^3 T + 24 T s_4 - 6\mu a_{1,3} + 2\rho a_{0,1}a_{2,1} + \rho {a_{1,1}}^2}{18\mu}. \tag{2.18}$$

The coefficients of the stream function can be explained with physical aspects, namely derivatives of viscous stress tensor, pressure and derivatives of pressure. The viscous stress tensor is

$$\tau_{ij} = \mu\left(\frac{\partial u_i}{\partial x_j} + \frac{\partial u_j}{\partial x_i}\right), \tag{2.19}$$

https://doi.org/10.1017/S0956792512000319 Published online by Cambridge University Press

where μ is the dynamic viscosity of the fluid. Applying (2.19) and the Navier–Stokes equations, one can verify the following relations:

$$\begin{aligned}
a_{0,1} &= u(0,0), \quad a_{1,1} = \frac{\tau_{xx}}{2\mu} = -\frac{\tau_{yy}}{2\mu},\\
a_{2,1} &= \frac{1}{4\mu}\frac{\partial \tau_{xx}}{\partial x} = -\frac{1}{4\mu}\frac{\partial \tau_{yy}}{\partial x},\\
a_{0,3} &= \frac{1}{12\mu}\left(\frac{\partial \tau_{xx}}{\partial x} + 2\frac{\partial \tau_{xy}}{\partial y}\right) = \frac{1}{12\mu}\left(-\frac{\partial \tau_{yy}}{\partial x} + 2\frac{\partial \tau_{xy}}{\partial y}\right),\\
a_{0,4} &= \frac{1}{12\mu}\left(\frac{\partial \tau_{xx}}{\partial x} - \frac{\partial \tau_{xy}}{\partial y}\right) = -\frac{1}{12\mu}\left(\frac{\partial \tau_{yy}}{\partial x} + \frac{\partial \tau_{xy}}{\partial y}\right),\\
a_{3,1} &= \frac{1}{12\mu}\frac{\partial^2 \tau_{xx}}{\partial x^2} = -\frac{1}{12\mu}\frac{\partial^2 \tau_{yy}}{\partial x^2},\\
a_{1,3} &= \frac{1}{12\mu}\frac{\partial^2 \tau_{xx}}{\partial y^2} = -\frac{1}{12\mu}\frac{\partial^2 \tau_{yy}}{\partial y^2},\\
\frac{\partial p}{\partial x} &= -\rho\, a_{0,1}a_{1,1} + 2\,\mu\, a_{2,1} + 6\,\mu\, a_{0,3},\\
\frac{\partial p}{\partial y} &= -2\,\rho\, {a_{0,1}}^2 s_2 + 4\,\mu\, s_2 a_{1,1} + 12\,\mu\, s_3 a_{0,1},
\end{aligned}$$

where μ, ρ, p are the viscosity, density and pressure respectively.

The interface will be transformed into a straight line after a coordinate change $x = \xi$, $y = \eta + f(x)$, and substituting this into the stream function we get

$$\begin{aligned}
\psi &= a_{0,1}\eta - s_2 a_{0,1}\eta^2 + a_{1,1}\xi\,\eta + a_{0,3}\eta^3 + (s_2 a_{1,1} - 3\,s_3 a_{0,1})\xi\,\eta^2\\
&\quad + (a_{2,1} - 2\,{s_2}^2 a_{0,1})\xi^2\eta + a_{1,3}\xi\,\eta^3 + a_{0,4}\eta^4 + (3\,a_{2,1}s_2 - 6\,s_4 a_{0,1}\\
&\quad + 6\,{s_2}^3 a_{0,1})\xi^2\eta^2 + (a_{3,1} - 2\,s_2 a_{0,1}s_3 + 2\,(s_2 a_{1,1} - 3\,s_3 a_{0,1})s_2)\xi^3\eta. \qquad (2.20)
\end{aligned}$$

2.1 Flow field as a nonlinear dynamical systems

Our problem can be written as a system of nonlinear differential equations using $\dot{\xi} = \frac{\partial \psi}{\partial \eta}$ and $\dot{\eta} = -\frac{\partial \psi}{\partial \xi}$.

The linear approximation of equation (2.20) is

$$\begin{pmatrix} \dot{\xi} \\ \dot{\eta} \end{pmatrix} = \begin{pmatrix} a_{0,1} \\ 0 \end{pmatrix} + \begin{pmatrix} a_{1,1} & -2s_2 a_{0,1} \\ 0 & -a_{1,1} \end{pmatrix} \begin{pmatrix} \xi \\ \eta \end{pmatrix}, \qquad (2.21)$$

with the Jacobian

$$J = \begin{pmatrix} a_{1,1} & -2s_2 a_{0,1} \\ 0 & -a_{1,1} \end{pmatrix}. \qquad (2.22)$$

If $a_{0,1} = 0$ in (2.21), the origin is a critical point. Substituting $a_{0,1} = 0$ in the Jacobian

https://doi.org/10.1017/S0956792512000319 Published online by Cambridge University Press

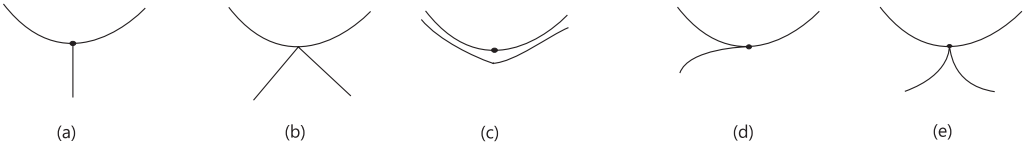

FIGURE 2. Streamlines near a critical point on the free surface. (a) Non-degenerate critical point for $a_{1,1} \neq 0$. Degenerate critical points (b) $a_{2,1}/a_{0,3} < 0$; (c) $a_{2,1}/a_{0,3} > 0$. These critical points were found by Brøns [3]. (d) $a_{0,1} = a_{1,1} = a_{2,1} = 0$, $a_{3,1} \neq 0, a_{0,3} \neq 0$. A dividing streamline, tangent to the free surface is also found in [5] with completely different boundary conditions, namely Navier conditions near a solid wall. (e) $a_{0,1} = a_{1,1} = a_{0,3} = 0$, $a_{2,1} \neq 0, a_{0,4} \neq 0$.

matrix we get

$$J = \begin{pmatrix} a_{1,1} & 0 \\ 0 & -a_{1,1} \end{pmatrix}. \tag{2.23}$$

We see that the origin is a saddle with eigenvalues $a_{1,1}$ and $-a_{1,1}$. The separatrix corresponding to $a_{1,1}$ is the interface, while the other separatrix is a dividing streamline which is orthogonal to the interface given by $\xi = 0$. The unstable direction is given by the eigenvector, $(0, 1)$. Thus, the origin has a separatrix in the direction $\xi = 0$, and the separation angle is $\theta = \frac{\pi}{2}$. This classical result was found by Brøns [3] and Lugt [14], and shows that if $a_{1,1} = \frac{\tau_{xx}}{2\mu} = -\frac{\tau_{yy}}{2\mu} \neq 0$, a separation line is perpendicular to the free surface. See Figure 2(a).

If $a_{0,1} = a_{1,1} = 0$, which means physically that $p_{0,0} = 2s_2 T$ from the normal stress condition (2.17), the origin is a degenerate critical point, since zero is a double eigenvalue of J. Also, the degenerate singularity occurs in a viscous flow if the pressure gradient $(\frac{\partial p}{\partial y})$ and the shear stress gradient $(\tau_{xx} = \tau_{yy} = 0)$ vanish simultaneously in the singular point. The corresponding stream function is given by

$$\psi = a_{2,1}\xi^2\eta + a_{0,3}\eta^3 + O(\xi^4, \eta^4). \tag{2.24}$$

Depending on the sign of the coefficients, there are two possibilities. If $a_{2,1}/a_{0,3} < 0$, two linear separatrices exist. If $a_{2,1}/a_{0,3} > 0$, there is no separatrix except at the interface. The saddle point has a dividing streamline in the direction $\eta = \pm\sqrt{-\frac{a_{2,1}}{a_{0,3}}}\xi$ and a streamline along the free surface ($\eta = 0$). The separation angle can be written in terms of shear stress gradient at the origin as

$$\tan\theta = \pm\sqrt{-\frac{a_{2,1}}{a_{0,3}}} = \pm\sqrt{-3\frac{\frac{\partial\tau_{xx}}{\partial x}}{\left(\frac{\partial\tau_{xx}}{\partial x} + 2\frac{\partial\tau_{xy}}{\partial y}\right)}} = \pm\sqrt{3\frac{\frac{\partial\tau_{yy}}{\partial x}}{\left(-\frac{\partial\tau_{yy}}{\partial x} + 2\frac{\partial\tau_{xy}}{\partial y}\right)}}. \tag{2.25}$$

Equation (2.25) shows that the separation angle of dividing streamlines depends on the shear stress gradient. See Figures 2(b) and (c). These types of degenerate critical points and their unfolding can be seen in [3].

https://doi.org/10.1017/S0956792512000319 Published online by Cambridge University Press

2.2 Non-simple degenerate critical points of order 4

Here we extend the degenerate conditions of case [3]. There are three classes of such cases that may arise:

$$(i)\quad a_{0,1} = a_{1,1} = a_{2,1} = 0,\quad a_{0,3} \neq 0, \left(\tau_{xx} = \tau_{yy} = \frac{\partial \tau_{xx}}{\partial x} = \frac{\partial \tau_{yy}}{\partial x} = 0,\ \frac{\partial \tau_{xy}}{\partial y} \neq 0\right),$$

$$(ii)\ a_{0,1} = a_{1,1} = a_{0,3} = 0,\quad a_{2,1} \neq 0, \left(\tau_{xx} = \tau_{yy} = \frac{\partial \tau_{xx}}{\partial x} + \frac{\partial \tau_{yy}}{\partial x} = 0,\ \frac{\partial \tau_{xx}}{\partial x} = \frac{\partial \tau_{yy}}{\partial x} \neq 0\right),$$

$$(iii)\ a_{0,1} = a_{1,1} = a_{0,3} = a_{2,1} = 0,\quad a_{3,1} \neq 0, a_{1,3} \neq 0, \left(\frac{\partial p}{\partial x} = \frac{\partial p}{\partial y} = 0, \frac{\partial^2 \tau_{xx}}{\partial x^2} \neq 0, \frac{\partial^2 \tau_{yy}}{\partial x^2} \neq 0\right).$$

If $a_{0,1} = a_{1,1} = a_{2,1} = 0$ but $a_{0,3} \neq 0$, which means physically that $p_{1,0} = 6s_3 T$ or $a_{0,3} = s_3 T/\mu$ from the normal stress condition (2.17), the corresponding stream function is given by

$$\psi = a_{3,1}\xi^3\eta + a_{1,3}\xi\,\eta^3 + a_{0,4}\eta^4 + a_{0,3}\eta^3. \tag{2.26}$$

To eliminate the fourth-order terms in (2.26) and for easy determination of the codimension, we use the idea of the normal form theory of [5] and [13] by choosing a different generating function. The new coordinates (ξ_*, η_*) are found from a canonical transformation defined by the generating function

$$S = \eta\xi_* + \sum_{i+j=3} s_{i,j}\eta^i \xi_*^j, \tag{2.27}$$

such that

$$\xi = \frac{\partial S}{\partial \eta},\quad \eta_* = \frac{\partial S}{\partial \xi_*}. \tag{2.28}$$

Solving (2.28) for ξ, η and including terms up to the second order yields

$$\xi = \xi_* + s_{1,2}\xi_*^2 + 2s_{2,1}\xi_*\eta_* + 3s_{3,0}\eta_*^2, \tag{2.29}$$

$$\eta = \eta_* - 3s_{0,3}\xi_*^2 - 2s_{1,2}\xi_*\eta_* - s_{2,1}\eta_*^2. \tag{2.30}$$

We require that the boundaries are preserved under the transformation, i.e. $\eta = 0$ is mapped to $\eta_* = 0$. This is achieved by taking $s_{0,3} = 0$ in (2.30). Inserting this transformation in (2.26) and truncating after the fourth-order order, we obtain

$$\begin{aligned}\psi = {} & a_{3,1}{\xi_*}^3\eta_* - 9\,a_{0,3}s_{0,3}{\xi_*}^2{\eta_*}^2 + \left(-6\,a_{0,3}s_{1,2} + a_{1,3}\right)\xi_*\,{\eta_*}^3 \\ & + \left(-3\,a_{0,3}s_{2,1} + a_{0,4}\right){\eta_*}^4 + a_{0,3}{\eta_*}^3.\end{aligned} \tag{2.31}$$

The $s_{i,j}$ are free for us to choose. With the choices

$$s_{2,1} = \frac{a_{0,4}}{3a_{0,3}}, s_{1,2} = \frac{a_{1,3}}{6a_{0,3}}, s_{0,3} = 0, \tag{2.32}$$

we eliminate a number of terms and get

$$\psi = a_{3,1}{\xi_*}^3\eta_* + a_{0,3}{\eta_*}^3. \tag{2.33}$$

https://doi.org/10.1017/S0956792512000319 Published online by Cambridge University Press

If $a_{0,3} \neq 0$ and $a_{3,1}/a_{0,3} < 0$, there is a cusp point on $\eta_* = 0$, see Figure 2(d). The condition $a_{0,3} \neq 0$ indicates that $\frac{1}{12\mu}(\frac{\partial \tau_{xx}}{\partial x} + 2\frac{\partial \tau_{xy}}{\partial y})$ and $\frac{1}{12\mu}(-\frac{\partial \tau_{yy}}{\partial x} + 2\frac{\partial \tau_{xy}}{\partial y})$ do not vanish at the singularity. The dividing streamlines are found as $\eta_* = \pm\sqrt{-\frac{a_{3,1}}{a_{0,3}}\xi^3}$ and $\xi_* = 0$. The ratio of $a_{3,1}/a_{0,3}$ can be expressed in local variables,

$$\frac{a_{3,1}}{a_{0,3}} = \frac{\frac{\partial^2 \tau_{xx}}{\partial x^2}}{\frac{\partial \tau_{xx}}{\partial x} + 2\frac{\partial \tau_{xy}}{\partial y}} = \frac{\frac{\partial^2 \tau_{yy}}{\partial x^2}}{\frac{\partial \tau_{yy}}{\partial x} - 2\frac{\partial \tau_{xy}}{\partial y}} \tag{2.34}$$

and will depend on the first- and second-order shear stress gradients. A degenerate pattern with a cusp is also found in [19], but in connections with completely different boundary conditions, namely Navier conditions near a solid wall.

In the second case, we consider the degeneracy of order 4, where $a_{0,1} = a_{1,1} = a_{0,3} = 0$ ($p_y = 0$) but $a_{2,1} \neq 0$ ($p_x \neq 0$), we have

$$\psi = a_{3,1}{\xi_*}^3\eta_* - a_{2,1}s_2{\xi_*}^2{\eta_*}^2 + a_{1,3}\xi_*{\eta_*}^3 + a_{0,4}{\eta_*}^4 + a_{2,1}{\xi_*}^2\eta_*. \tag{2.35}$$

We proceed as in case ($a_{0,3} \neq 0$) to eliminate ($\xi_*{\eta_*}^3$ and $\xi_*^2{\eta_*}^2$) from the stream function (2.35) by choosing

$$s_{3,0} = -\frac{a_{1,3}}{6a_{2,1}}, s_{2,1} = \frac{s_2}{3}. \tag{2.36}$$

With these simplification, we have

$$\psi = a_{2,1}{\xi_*}^2\eta_* + a_{0,4}{\eta_*}^4 + a_{3,1}{\xi_*}^3\eta_*. \tag{2.37}$$

Further reduction is possible by a quadratic transformation, see for example [19]. Substituting the transformation $\xi_* \to \xi_* - \frac{a_{3,1}}{3a_{2,1}}\xi_*^2$ into (2.37) gives

$$\psi = \eta_*(a_{2,1}{\xi_*}^2 + a_{0,4}{\eta_*}^3). \tag{2.38}$$

Possible separatrices of the point are given by $\psi = 0$, which gives

$$\eta_* = 0, \xi_* = \pm\sqrt{-\frac{a_{0,4}}{a_{2,1}}\eta_*^3}, \tag{2.39}$$

or expressed in physical terms

$$\eta_* = 0, \xi_* = \pm\sqrt{3\frac{\frac{\partial \tau_{xx}}{\partial x} - \frac{\partial \tau_{xy}}{\partial y}}{\frac{\partial \tau_{xx}}{\partial x}}\eta_*^3} = \pm\sqrt{3\frac{\frac{\partial \tau_{yy}}{\partial x} + \frac{\partial \tau_{xy}}{\partial y}}{\frac{\partial \tau_{yy}}{\partial x}}\eta_*^3}. \tag{2.40}$$

It shows a cusp separatrix on the free surface, see Figure 2(e). This critical point is also seen by Deliceoğlu and Gürcan [8] under the symmetric condition about a straight line away from boundaries.

In the third case, further degenerate flow patterns are obtained by extending degeneracy taking $a_{0,1} = a_{1,1} = a_{2,1} = a_{0,3} = 0$ in equation (2.20), which means that $s_3 = 0$ from the normal stress condition (2.17) (in other words, the interface must be a parabola) in the

https://doi.org/10.1017/S0956792512000319 Published online by Cambridge University Press

stream function. Substituting the above condition in the stream function (2.20), we get

$$\psi = \eta(a_{31}\xi^3 + a_{13}\xi\eta^2 + a_{04}\eta^3). \tag{2.41}$$

There are three terms of order 3. To find the degenerate flow patterns we should reduce the number of parameters. This will be achieved by using the Navier–Stokes equation. From the vorticity transport equation we get the following relation of the stream function:

$$\upsilon\nabla^4\psi = \frac{\partial\nabla^2\psi}{\partial t} + \frac{\partial\psi}{\partial y}\frac{\partial}{\partial x}(\nabla^2\psi) - \frac{\partial\psi}{\partial x}\frac{\partial}{\partial y}(\nabla^2\psi), \tag{2.42}$$

where υ is the kinematic viscosity. Inserting the expansion (2.8) and collecting terms of the same order in x, y gives a series of algebraic equations for $a_{i,j}$. The equations of order 0 and 1 are given by

$$\begin{aligned}
x^0y^0 &: \upsilon(72\,s_2{}^3a_{0,1} - 32\,a_{2,1}s_2 - 72\,s_4a_{0,1} - 48\,s_3a_{1,1} + 24\,a_{0,4} - 24\,a_{0,3}s_2)\\
&\quad = a_{0,1}(-8\,s_2a_{1,1} - 12\,s_3a_{0,1}),\\
x^0y^1 &: a_{0,1}(6\,a_{3,1} + 6\,a_{1,3}) - 2\,s_2a_{0,1}(-8\,s_2a_{1,1} - 12\,s_3a_{0,1}) - a_{1,1}(2\,a_{2,1} + 6\,a_{0,3}) = 0,\\
x^1y^0 &: a_{0,1}(-36\,s_3a_{1,1} + 48\,s_2{}^3a_{0,1} - 28\,a_{2,1}s_2 - 48\,s_4a_{0,1} - 12\,a_{0,3}s_2) + a_{1,1}(-8\,s_2a_{1,1}\\
&\quad -12\,s_3a_{0,1}) + 2\,s_2a_{0,1}(2\,a_{2,1} + 6\,a_{0,3}) = 0.
\end{aligned} \tag{2.43}$$

By using (2.43) and the assumption $a_{0,1} = a_{1,1} = a_{2,1} = a_{0,3} = 0$, we get $a_{0,4} = 0$ and the stream function (2.41) becomes

$$\psi = \eta(a_{3,1}\xi^3 + a_{1,3}\xi\eta^2). \tag{2.44}$$

Theorem 2.1 *Let $a_{0,1}, a_{1,1}, a_{2,1}$ and $a_{0,3}$ become zero. Assuming the non-degeneracy conditions $a_{1,3} \neq 0, a_{3,1} \neq 0$ hold, then the normal form of order 4 for the stream function (2.8) is*

$$\psi = \eta(a_{3,1}\xi^3 + a_{1,3}\xi\eta^2). \tag{2.45}$$

From the theorem, the local flow topology in the neighbourhood of the non-simple degenerate critical point can be easily obtained. Possible separatrices (dividing streamlines) of the critical point are given by $\psi = 0$, that is

$$\xi = 0, \quad \eta = 0, \quad \eta = \pm\sqrt{-\frac{a_{3,1}}{a_{1,3}}}\,\xi. \tag{2.46}$$

If $\frac{a_{3,1}}{a_{1,3}} = \frac{\frac{\partial^2\tau_{xx}}{\partial x^2}}{\frac{\partial^2\tau_{xx}}{\partial y^2}} > 0$, there are three separatrices (see Figure 3(a)). If $\frac{a_{3,1}}{a_{1,3}} = \frac{\frac{\partial^2\tau_{xx}}{\partial x^2}}{\frac{\partial^2\tau_{xx}}{\partial y^2}} < 0$, there are five separatrices from a single saddle, and this case is denoted by a topological saddle (see Figure 3(b)). Equation (2.16) for pressure is equivalent to constant under the condition $a_{0,1} = a_{1,1} = a_{2,1} = a_{0,3} = 0$ and $a_{3,1} + a_{1,3} = 0$. It follows that situation (b) in Figure (3) is possible under the constant pressure condition.

https://doi.org/10.1017/S0956792512000319 Published online by Cambridge University Press

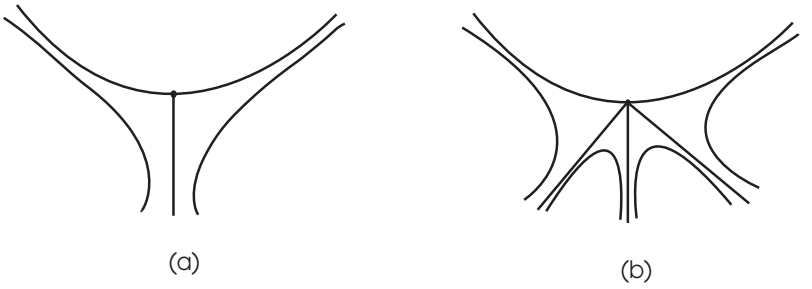

FIGURE 3. Non-simple degenerate critical points. (a) $\frac{a_{3,1}}{a_{1,3}} > 0$, (b) $\frac{a_{3,1}}{a_{1,3}} < 0$.

2.3 Bifurcation of non-simple degenerate critical points of order 4

The degenerate flow patterns (Figure 2) obtained in the previous section will appear only when some coefficients of the stream function are zero. In this section, to determine all possible bifurcations close to non-simple degenerate critical points, a small perturbation of these coefficients known as the bifurcation value in the stream function is considered. The idea of the normal form theory of Brøns [5] is used by choosing a different generating function preserving kinematic boundary conditions (a), (b) and (c).

2.3.1 *Bifurcation of degenerate critical point for* $a_{0,1} = a_{1,1} = a_{2,1} = 0, a_{3,1} \neq 0$

To study the bifurcations close to the non-simple degenerate critical points, we introduce small parameters $\epsilon_1 = a_{0,1}, \epsilon_2 = a_{1,1}, \epsilon_3 = a_{2,1}$ and by substituting these parameters into the stream function (2.20) we obtain

$$\begin{aligned}\psi = {} & \left(a_{3,1} + 2\,(s_2\epsilon_2 - 3\,s_3\epsilon_1)\,s_2 - 2\,s_2\epsilon_1 s_3\right)\xi^3\eta + (3\,\epsilon_3 s_2 + 6\,{s_2}^3\epsilon_1 \\ & -6\,s_4\epsilon_1)\xi^2\eta^2 + a_{1,3}\xi\,\eta^3 + a_{0,4}\eta^4 + \left(\epsilon_3 - 2\,{s_2}^2\epsilon_1\right)\xi^2\eta + (s_2\epsilon_2 \\ & -3\,s_3\epsilon_1)\xi\,\eta^2 + a_{0,3}\eta^3 + \epsilon_2\xi\,\eta - s_2\epsilon_1\eta^2 + \epsilon_1\eta. \end{aligned} \tag{2.47}$$

Now we apply normal form transformations to simplify some terms of the stream function (2.47), but include small parameters in the transformations. The new coordinates (ξ_*, η_*) are found from a canonical transformation defined by the generating function

$$S = \eta\xi_* + \sum_{i+j+k+l+m=3} s_{i,j,k,l,m}\eta^i\xi_*^j\epsilon_1^k\epsilon_2^l\epsilon_3^m, \tag{2.48}$$

such that

$$\xi = \frac{\partial S}{\partial \eta}, \quad \eta_* = \frac{\partial S}{\partial \xi_*}. \tag{2.49}$$

The method for finding the normal form of bifurcation of degenerate critical points proceeds as in previous studies ([5, 11]). We omit computation steps and only give the following transformed stream function:

$$\psi = \eta_*(\widetilde{a}_{0,1} + \widetilde{a}_{0,2}\eta_* + \widetilde{a}_{1,1}\xi_* + a_{0,3}\eta_*^2 + a_{3,1}\xi_*^3), \tag{2.50}$$

https://doi.org/10.1017/S0956792512000319 Published online by Cambridge University Press

where

$$\widetilde{a}_{0,1} = \epsilon_1 + O_2(\epsilon_1, \epsilon_2, \epsilon_3), \quad \widetilde{a}_{0,2} = \left(-s_2 - \frac{a_{0,4}}{3a_{0,3}}\right)\epsilon_1 + O_2(\epsilon_1, \epsilon_2, \epsilon_3), \tag{2.51}$$

$$\widetilde{a}_{1,1} = -\frac{a_{1,3}}{3a_{0,3}}\epsilon_1 + \epsilon_2 + O_2(\epsilon_1, \epsilon_2, \epsilon_3). \tag{2.52}$$

Note that $\widetilde{a}_{0,1}, \widetilde{a}_{0,2}$ and $\widetilde{a}_{1,1}$ can be expressed as linear combinations of two small parameters ϵ_1 and ϵ_2 if the terms of higher order than 2 are neglected. Hence, the stream function depends on two small parameters ϵ_1 and ϵ_2. A final simplification can be obtained by first dividing ψ by $a_{0,3}$ corresponding to scaling the time and then scale ξ_* by the substitution $\xi_* \to \sqrt[3]{\frac{a_{0,3}}{a_{3,1}}}\xi_*$ to obtain

$$\psi = \eta_*(\overline{\mu}_1 + a\overline{\mu}_1\eta_* + \overline{\mu}_3\xi_* + \eta_*^2 + \xi_*^3) + O(\xi_*, \eta_*)^5, \tag{2.53}$$

where $\overline{\mu}_1, \overline{\mu}_3$ are the new small parameters depending on ϵ_1, ϵ_2, and a is a small constant. The reader will note that the normal form (2.53) is almost the same as the normal form of equation (55) in [19]. The flow patterns and their bifurcations are exactly the same as in [19], so the relevant computations and bifurcation diagrams are omitted.

Here we focus on the case of $\widetilde{a}_{0,1}$, $\widetilde{a}_{0,2}$ and $\widetilde{a}_{1,1}$ as a linear combination of three small parameters ϵ_1, ϵ_2 and ϵ_3 by including higher order terms in equations (2.51) and (2.52). Now the stream function depends on three small parameters ϵ_1, ϵ_2 and ϵ_3. Once again, dividing ψ by $a_{0,3}$ corresponding to scaling the time and then scale ξ_* by the substitution $\xi_* \to \sqrt[3]{\frac{a_{0,3}}{a_{3,1}}}\xi_*$ to obtain

$$\psi = \eta_*(\overline{\mu}_1 + \overline{\mu}_2\eta_* + \overline{\mu}_3\xi_* + \eta_*^2 + \xi_*^3) + O((\xi_*, \eta_*))^5, \tag{2.54}$$

where $\overline{\mu}_1, \overline{\mu}_2, \overline{\mu}_3$ are the new small parameters depending on $\epsilon_1, \epsilon_2, \epsilon_3$.

Proceeding as above, in the general case (re-labeling the coordinates back to x, y) one obtains the following.

Theorem 2.2 *Let $a_{0,1}, a_{1,1}$ and $a_{2,1}$ be small parameters. Assuming the non-degeneracy conditions $a_{0,3} \neq 0, a_{3,1} \neq 0$ are satisfied, then the normal form of order 4 for the stream function (2.8) is*

$$\psi = y(\mu_1 + \mu_2 y + \mu_3 x + y^2 + x^3) + O((x, y))^5, \tag{2.55}$$

where μ_1, μ_2 and μ_3 are small transformed parameters.

The corresponding dynamical systems with codimension three are

$$\begin{aligned} \dot{x} &= \mu_1 + 2\mu_2 y + \mu_3 x + 3y^2 + x^3, \\ \dot{y} &= -y(\mu_3 + 3x^2). \end{aligned} \tag{2.56}$$

The critical point on the free surface ($y = 0$) is $\mu_1 + \mu_3 x + x^3 = 0$, and there is a bifurcation curve for $4\mu_3^3 + 27\mu_1^2 = 0$, which divides parameter plane into two regions. In one of these

https://doi.org/10.1017/S0956792512000319 Published online by Cambridge University Press

regions there are three fixed points, while in the other there is a single fixed point. Crossing these curves, a separation bubble on the free surface is created or destroyed.

Off the axis ($y \neq 0$), local bifurcations occur when

$$\mu_3 + 3x^2 = 0 \quad \text{and} \quad \mu_1 + 2\mu_2 y + \mu_3 x + 3y^2 + x^3 = 0.$$

Combining these, one obtains the following four critical points away from the free surface:

$$A\left(\frac{\sqrt{-3\,\mu_3}}{3}, -\frac{\mu_2}{3} + \frac{\sqrt{\Delta_1}}{9}\right), \quad B\left(\frac{\sqrt{-3\,\mu_3}}{3}, -\frac{\mu_2}{3} - \frac{\sqrt{\Delta_1}}{9}\right),$$
$$C\left(-\frac{\sqrt{-3\,\mu_3}}{3}, -\frac{\mu_2}{3} + \frac{\sqrt{\Delta_2}}{9}\right), \quad D\left(-\frac{\sqrt{-3\,\mu_3}}{3}, -\frac{\mu_2}{3} - \frac{\sqrt{\Delta_2}}{9}\right),$$

where

$$\Delta_1 = 9\,{\mu_2}^2 - 27\,\mu_1 - 6\,\mu_3\sqrt{3}\sqrt{-\mu_3}, \quad \Delta_2 = 9\,{\mu_2}^2 - 27\,\mu_1 + 6\,\mu_3\sqrt{3}\sqrt{-\mu_3}. \tag{2.57}$$

The types of the critical point can be determined by the sign of the determinant of the Jacobian matrix $|J| = 6\,yx(2\,\mu_2 + 6\,y) - (\mu_3 + 3\,x^2)^2$. Evaluating $|J|$ at singular points, one finds $A(\frac{\sqrt{-3\,\mu_3}}{3}, -\frac{\mu_2}{3} + \frac{\sqrt{\Delta_1}}{9})$ and $D(-\frac{\sqrt{-3\,\mu_3}}{3}, -\frac{\mu_2}{3} - \frac{\sqrt{\Delta_2}}{9})$ are centres, while other singular points such as $B(\frac{\sqrt{-3\,\mu_3}}{3}, -\frac{\mu_2}{3} - \frac{\sqrt{\Delta_1}}{9})$ and $C(-\frac{\sqrt{-3\,\mu_3}}{3}, -\frac{\mu_2}{3} + \frac{\sqrt{\Delta_2}}{9})$ are saddle points for $\mu_2 < 0$. The bifurcation which occurs away from the boundaries is the merging and disappearance of a saddle and a centre and denotes a cusp bifurcation, which is labelled by C_1 and C_2 in Figure 4. This occurs when $\Delta_1 = 0$ or $\Delta_2 = 0$. In addition to these bifurcation curves, the stream function value of the interior saddle point can take the same value as the critical points on the free surface. Such a configuration appears when $\psi(C) = 0$. From this we find that bifurcation curve is given by

$$\frac{1}{729}\left(3\,\mu_2 - \sqrt{\Delta_2}\right)\left(-81\,\mu_1 + 18\,{\mu_2}^2 - 3\,\mu_2\sqrt{\Delta_2} + 18\,\mu_3\sqrt{3}\sqrt{-\mu_3} - \Delta_2\right) = 0, \tag{2.58}$$

which is labeled by G_1 in Figure 4. In order to obtain the equation of the heteroclinic bifurcation curve, we need $\psi(B) = \psi(C)$. The calculation shows

$$1/27\,{\mu_2}^2\sqrt{\Delta_1} - \frac{4}{27}\,\mu_2\mu_3\sqrt{3}\sqrt{-\mu_3} - 1/9\,\sqrt{\Delta_1}\mu_1 - \frac{2}{81}\,\sqrt{\Delta_1}\mu_3\sqrt{3}\sqrt{-\mu_3}$$
$$-\frac{1}{729}\,{\Delta_1}^{3/2} + 1/27\,{\mu_2}^2\sqrt{\Delta_2} - 1/9\,\sqrt{\Delta_2}\mu_1 + \frac{2}{81}\,\sqrt{\Delta_2}\mu_3\sqrt{3}\sqrt{-\mu_3} - \frac{1}{729}\,{\Delta_2}^{3/2} = 0, \tag{2.59}$$

which is labeled by G_2 in Figure 4.

A series of flow structures is represented in the (μ_1, μ_3) space as shown in Figure 4. A topology of type (1) shows a single dividing streamline on the free surface. By varying of the parameter space, type (2) is obtained by applying a cusp point bifurcation in the flow. Then we see that this cusp critical point unfolds into a homoclinic pattern. The flow patterns ((14), (17) and (19)) indicate the possible cusp point bifurcation in the bifurcation diagram. Going to region (4), we approach bifurcation (3) where a separation bubble on

https://doi.org/10.1017/S0956792512000319 Published online by Cambridge University Press

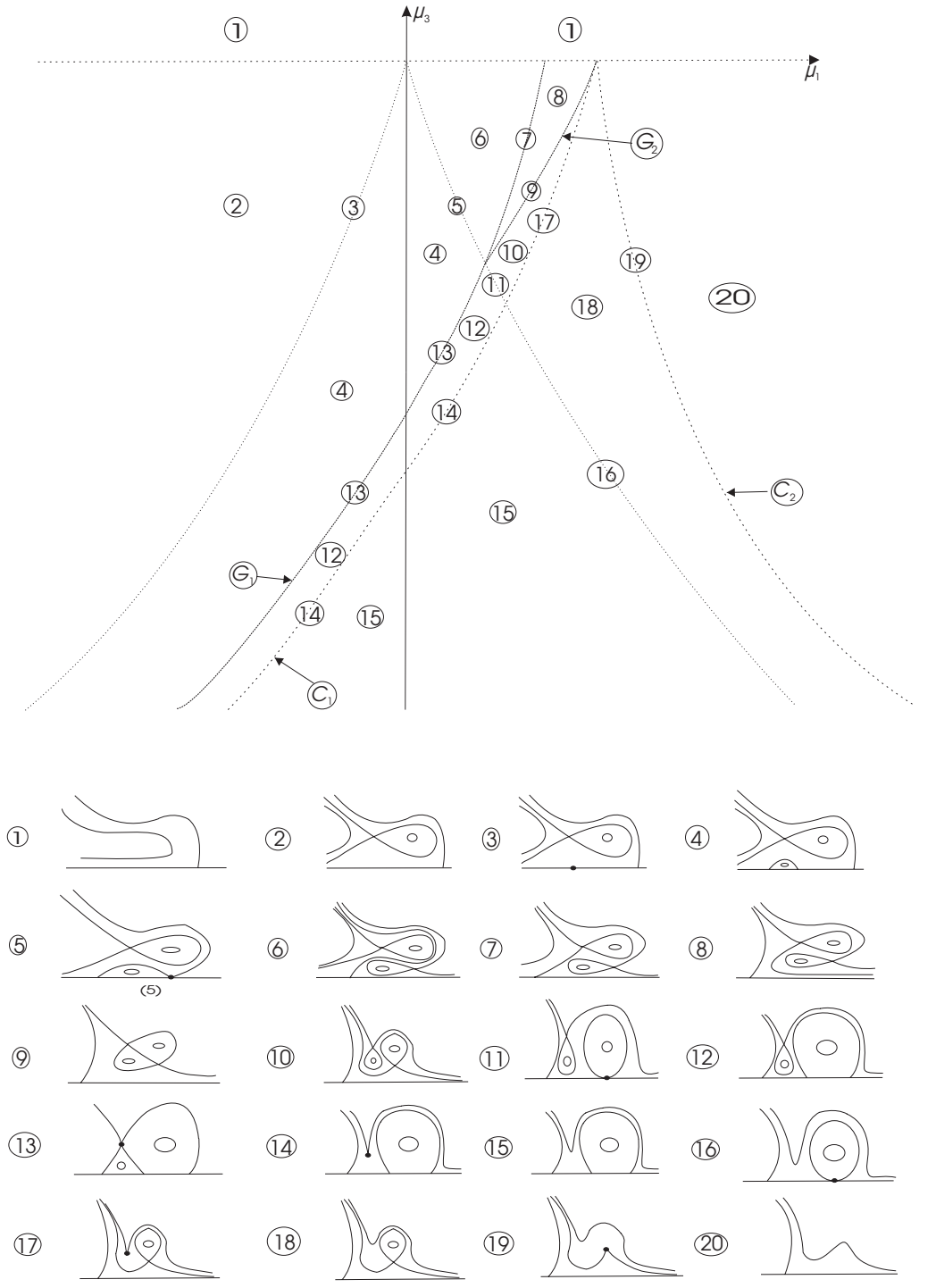

FIGURE 4. Bifurcation diagram for the normal form (2.55) in the (μ_1, μ_2, μ_3) parameter space with $\mu_2 < 0$.

https://doi.org/10.1017/S0956792512000319 Published online by Cambridge University Press

the free surface is created. Crossing this curve will unfold this degenerate point similar to type (4). Consequently, the flow region (4) in Figure 4 contains a separation bubble on the free surface with the homoclinic orbit. Going from region (4) to region (6) a bubble merging bifurcation (5) is crossed, indicating that the two saddle points on the free surface coalesce. Entering region (8) from (6), the curve G_1 is passed, on which a saddle connection exists between the saddle on the free surface and the saddle in the flow as shown in flow pattern (7).

The flow pattern (9) in Figure 4 deserves further consideration since the interaction of two vortices with opposite rotation occurs only near the non-simple degenerate critical point. Two topologically different flow structures (8) and (10) appear in the same area, but this is possible only in the event of global bifurcation (9) which divides the region into subregions (8) and (10). Examining the changes in the structure near the free surface, we encounter a vortex ring bifurcation (11) which attaches to the free surface at a singular point. This bifurcation causes the creation of a separation bubble with a homoclinic orbit, see (12). Other important pattern arises from the global bifurcation (13) between the separation bubble on the free surface and an in-flow vortex ring. Entering region (15) from (12), the curve C_1 is passed on which the centre–saddle pair has disappeared. The flow pattern (18) is obtained by applying a bubble merging bifurcation (16) or a cusp point bifurcation (17) in the flow.

2.3.2 *Bifurcation of degenerate critical point for* $a_{0,1} = a_{1,1} = a_{0,3} = 0, a_{2,1} \neq 0$

As we mentioned at the beginning of Section (2.3.1), we use the generating function and a near-identity quadratic transformation to obtain the normal form of the stream function. Here we consider small parameters $\epsilon_1 = a_{0,1}, \epsilon_2 = a_{1,1}, \epsilon_3 = a_{0,3}$, and substituting these parameters into the stream function (2.20) we find

$$\begin{aligned}\psi = {} & \left(a_{3,1} + 2\,(s_2\epsilon_2 - 3\,s_3\epsilon_1)\,s_2 - 2\,s_2\epsilon_1 s_3\right)\xi^3\eta + (3\,a_{2,1}s_2 + 6\,{s_2}^3\epsilon_1 \\ & - 6\,s_4\epsilon_1)\xi^2\eta^2 + a_{1,3}\xi\,\eta^3 + a_{0,4}\eta^4 + \left(a_{2,1} - 2\,{s_2}^2\epsilon_1\right)\xi^2\eta + (s_2\epsilon_2 \\ & - 3\,s_3\epsilon_1)\xi\,\eta^2 + \epsilon_3\eta^3 + \epsilon_2\xi\,\eta - s_2\epsilon_1\eta^2 + \epsilon_1\eta, \end{aligned} \tag{2.60}$$

where $\epsilon_1 = a_{0,1}, \epsilon_2 = a_{1,1}$ and $\epsilon_3 = a_{0,3}$ are small parameters.

By choosing

$$s_{21000} = -s_2, s_{11100} = \frac{2{s_2}^2}{a_{2,1}}, s_{11010} = \frac{a_{3,1}}{2{a_{2,1}}^2}, s_{20100} = \frac{3s_3}{4a_{2,1}} \tag{2.61}$$

and setting the remaining coefficients in the generating function S equal to zero, equation (2.60) becomes

$$\begin{aligned}\psi = {} & a_{3,1}{\xi_*}^3\eta_* + a_{0,4}{\eta_*}^4 + \left(\frac{a_{3,1}\epsilon_2}{2a_{2,1}} + a_{2,1}\right){\xi_*}^2\eta_* + \left(\epsilon_3 - 2\,{s_2}^2\epsilon_1 - \frac{\epsilon_2 a_{1,3}}{2a_{2,1}}\right){\eta_*}^3 \\ & + \epsilon_2\xi_*\,\eta_* + \left(\left(\frac{3s_3}{2a_{2,1}} + \frac{s_2 a_{3,1}}{{a_{2,1}}^2}\right)\epsilon_1\epsilon_2 + 4\,\frac{{s_2}^3{\epsilon_1}^2}{a_{2,1}}\right){\eta_*}^2 \\ & + \left(-2\,\frac{{s_2}^2{\epsilon_1}^2}{a_{2,1}} - \frac{a_{3,1}\epsilon_1\epsilon_2}{{2a_{2,1}}^2} + \epsilon_1\right)\eta_*. \end{aligned} \tag{2.62}$$

https://doi.org/10.1017/S0956792512000319 Published online by Cambridge University Press

By changing $\xi_* \to \xi_* - \frac{a_{3,1}}{2a_{2,1}}\xi_*^2$, then (2.62) takes the form

$$\psi = a_{0,4}{\eta_*}^4 + a_{2,1}{\xi_*}^2\eta_* + \left(\epsilon_3 - 2\,{s_2}^2\epsilon_1 - \frac{\epsilon_2 a_{1,3}}{2a_{2,1}}\right){\eta_*}^3 + \epsilon_2\xi_*\,\eta_* + \left(\left(\frac{3s_3}{2a_{2,1}} + \frac{s_2 a_{3,1}}{{a_{2,1}}^2}\right)\epsilon_1\epsilon_2 + 4\,\frac{{s_2}^3{\epsilon_1}^2}{a_{2,1}}\right){\eta_*}^2 + \left(-2\,\frac{{s_2}^2{\epsilon_1}^2}{a_{2,1}} - \frac{a_{3,1}\epsilon_1\epsilon_2}{2{a_{2,1}}^2} + \epsilon_1\right)\eta_*. \tag{2.63}$$

Translation of the origin will remove the terms of the next highest degree $(\xi_*\eta_*)$ in the stream function by replacing ξ_* by $\xi_* + \xi_0$, where $\xi_0 = -\frac{\epsilon_2}{2a_{2,1}}$, then we obtain

$$\psi = a_{0,4}{\eta_*}^4 + a_{2,1}{\xi_*}^2\eta_* + \left(\epsilon_3 - 2\,{s_2}^2\epsilon_1 - \frac{\epsilon_2 a_{1,3}}{2a_{2,1}}\right){\eta_*}^3 + \left(\left(\frac{3s_3}{2a_{2,1}} + \frac{s_2 a_{3,1}}{{a_{2,1}}^2}\right)\epsilon_1\epsilon_2 + 4\,\frac{{s_2}^3{\epsilon_1}^2}{a_{2,1}}\right){\eta_*}^2 + \left(-\frac{{\epsilon_2}^2}{4a_{2,1}} - 2\,\frac{{s_2}^2{\epsilon_1}^2}{a_{2,1}} - \frac{a_{3,1}\epsilon_1\epsilon_2}{2{a_{2,1}}^2} + \epsilon_1\right)\eta_*. \tag{2.64}$$

A final simplification can be obtained by first dividing ψ by $\widetilde{a}_{2,1}$ corresponding to scaling the time and then scaling η_* by the substitution $\eta_* \to \sqrt[3]{\frac{\widetilde{a}_{2,1}}{a_{0,4}}}\eta_*$ to obtain

$$\psi = \eta_*(\xi_*^2 + b_0 + b_1\eta_* + b_2\eta_*^2 + \eta_*^3) + O((\xi_*, \eta_*)^5. \tag{2.65}$$

Proceeding as above, in the general case (re-labeling the coordinates back to x, y) one obtains the following.

Theorem 2.3 *Let $a_{0,1}, a_{1,1}$ and $a_{0,3}$ be small parameters. Assuming the non-degeneracy conditions $a_{2,1} \neq 0, a_{0,4} \neq 0$ are satisfied, then the normal form of order 4 for the stream function (2.8) is*

$$\psi = y(x^2 + b_0 + b_1 y + b_2 y^2 + y^3) + O((x, y)^5, \tag{2.66}$$

where b_0, b_1 and b_2 are small transformed parameters.

The reader will note that the normal form (2.66) is almost the same as the normal form of (28) in [8]. The flow patterns and their bifurcations are exactly the same as in [8], so the relevant computations are omitted and bifurcation diagrams are illustrated in Figure 5.

There exist three different kinds of bifurcation curves in Figure 5, which are labeled by B, C, G. In the first kind, there is a bubble creation, that is, with a centre away from the boundaries and two on-free surface saddles which are connected by heteroclinic trajectories (see Figure 5(d)). In the second kind, a cusp bifurcation, which occurs away from the free surface, is the merging and disappearance of a saddle and a centre (see Figure 5(c)). In addition to these bifurcation curves, the stream function value of the interior saddle point can take the same value as the critical points on the free surface. It yields a global bifurcation curve, which is labeled by G in the bifurcation diagram. New flow patterns are found in which the saddle of the homoclinic pattern is connected

https://doi.org/10.1017/S0956792512000319 Published online by Cambridge University Press

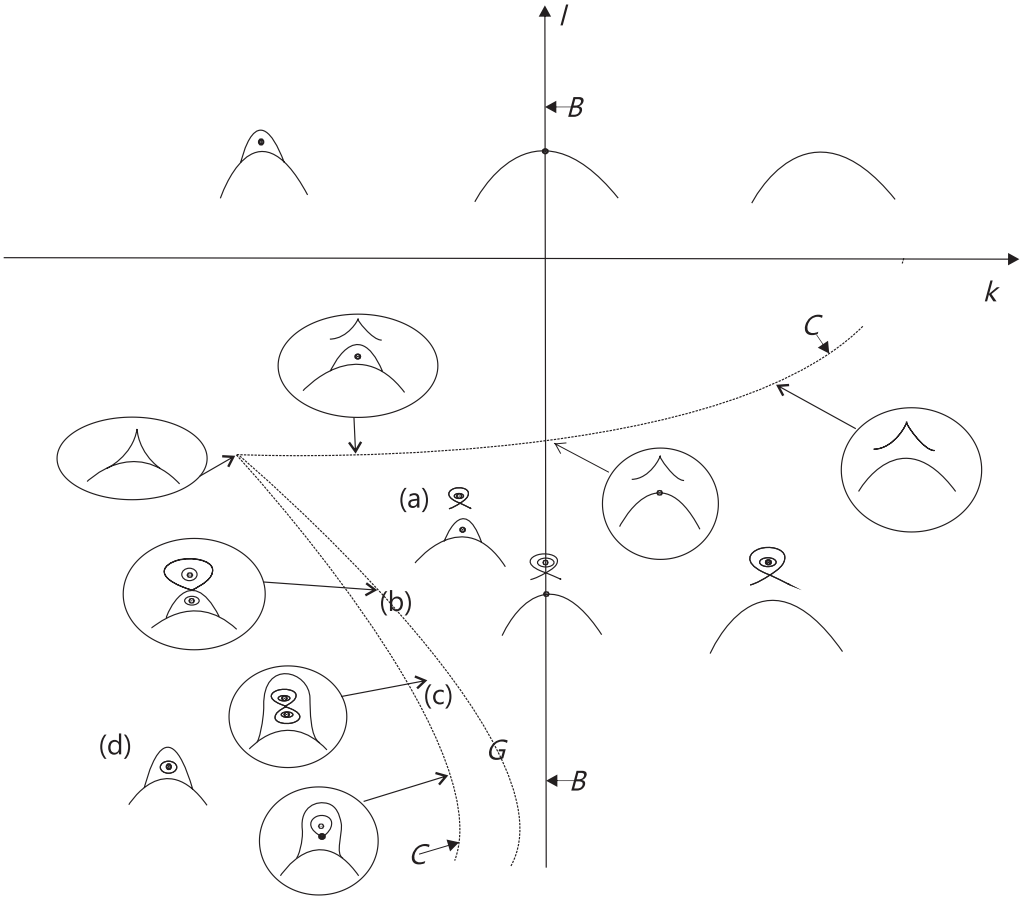

FIGURE 5. Bifurcation diagram for the fourth-order normal form (2.66) with $b_1 > 0$.

by a separation bubble on the free surface (see Figure 5(b)). These patterns can also be observed in a reverse double-film-fed roll coating nip as an application of the theoretical framework.

2.3.3 *Bifurcation of degenerate critical point for* $a_{0,1} = a_{1,1} = a_{2,1} = a_{0,3} = 0$

A normal form transformation for the degenerate critical point under the condition $a_{0,1} = a_{1,1} = a_{2,1} = a_{0,3} = 0$ is quite similar to the one made for the degenerate case ($a_{0,1} = a_{1,1} = a_{2,1} = 0$ or $a_{0,1} = a_{1,1} = a_{0,3} = 0$). As in that situation, analogous changes of parameters and variables show that our map can be transformed into the form

$$\psi = y(\mu_1 + \mu_2 x + \mu_3 y^2 + \omega x y^2 + x^3), \tag{2.67}$$

where μ_1, μ_2 and μ_3 are small transformed parameters. For this reason, we define small parameters $\epsilon_1 = a_{01}, \epsilon_2 = a_{11}, \epsilon_3 = a_{21}, \epsilon_4 = a_{03}$, and substituting these parameters into

https://doi.org/10.1017/S0956792512000319 Published online by Cambridge University Press

the stream function (2.20) we obtain

$$\begin{aligned}\psi &= (a_{3,1} - 2\,s_2\epsilon_1 s_3 + 2\,(s_2\epsilon_2 - 3\,s_3\epsilon_1)s_2)\xi^3\eta + (3\,\epsilon_3 s_2 - 6\,s_4\epsilon_1 + 6\,{s_2}^3\epsilon_1)\xi^2\eta^2 \\ &+ a_{1,3}\xi\eta^3 - \frac{1}{6v}(-6\,v s_3\epsilon_2 + 18\,v{s_2}^3\epsilon_1 - 18\,v s_4\epsilon_1 - 6\,v\epsilon_4 s_2 + \epsilon_1 s_2\epsilon_2 + 3\,s_3{\epsilon_1}^2)\eta^4 \\ &+(-2\,{s_2}^2\epsilon_1 + \epsilon_3)\xi^2\eta + (s_2\epsilon_2 - 3\,s_3\epsilon_1)\xi\eta^2 + \epsilon_4\eta^3 + \epsilon_2\xi\eta - s_2\epsilon_1\eta^2 + \epsilon_1\eta.\end{aligned} \tag{2.68}$$

We proceed as in (2.3.1) and (2.3.2) to simplify the fourth order terms of the stream function (2.68). We omit the detail computations and only give the result by the following theorem.

Theorem 2.4 *Let $a_{0,1}, a_{1,1}, a_{2,1}$ and $a_{0,3}$ be small parameters. Assuming the non-degeneracy conditions $a_{1,3} \neq 0$ and $a_{3,1} \neq 0$ are satisfied, then the normal form of order 4 for the stream function (2.8) is*

$$\psi = y(\mu_1 + \mu_2 x + \mu_3 y^2 + \omega x y^2 + x^3), \tag{2.69}$$

where μ_1, μ_2 and μ_3 are small transformed parameters.

Using the normal form (2.69) with codimension three, the corresponding dynamical system,

$$\begin{aligned}\dot{x} &= \mu_1 + \mu_2 x + 3\mu_3 y^2 + 3\omega x y^2 + x^3, \\ \dot{y} &= -y(\mu_2 + \omega y^2 + 3x^2),\end{aligned} \tag{2.70}$$

with the Jacobian

$$\mathbf{J} = \begin{pmatrix} \mu_2 + 3\omega y^2 + 3x^2 & 6\mu_3 y + 6\omega x y \\ -6xy & -\mu_2 - 3\omega y^2 - 3x^2 \end{pmatrix},$$

can be analysed by using the description of Gürcan *et al.* [12]. When $det(J) = 0$ on the free surface, the bifurcation occurs for

$$\begin{aligned}\mu_1 + \mu_2 x + x^3 &= 0, \\ \mu_2 + 3x^2 &= 0.\end{aligned} \tag{2.71}$$

By eliminating x one finds

$$\left(\frac{\mu_2}{3}\right)^3 = -\left(\frac{\mu_1}{2}\right)^2, \tag{2.72}$$

which forms a bifurcation set labelled by F_1. Away from the free surface ($y \neq 0$), we get

$$\begin{aligned}y^2 &= -3\,\frac{x^2}{\omega} - \frac{\mu_2}{\omega}, \\ \mu_1 &+ \mu_2 x + 3\,\mu_3 y^2 + 3\,\omega\, x y^2 + x^3 = 0.\end{aligned}$$

By eliminating y^2, one finds

$$\mu_1 - 3\,\frac{\mu_3\mu_2}{\omega} - 2\,\mu_2 x - 9\,\frac{\mu_3 x^2}{\omega} - 8\,x^3 = 0 \tag{2.73}$$

https://doi.org/10.1017/S0956792512000319 Published online by Cambridge University Press

giving the local bifurcation which occurs for $\omega = 1$

$$192\,\mu_2{}^3 + 5589\,\mu_3{}^2\mu_2{}^2 + 6561\,\mu_2\mu_3{}^4 - 5832\,\mu_3\mu_2\mu_1 + 1296\,\mu_1{}^2 - 2187\,\mu_1\mu_3{}^3 = 0, \quad (2.74)$$

and for $\omega = -1$

$$192\,\mu_2{}^3 + 5589\,\mu_3{}^2\mu_2{}^2 + 6561\,\mu_2\mu_3{}^4 + 5832\,\mu_3\mu_2\mu_1 + 1296\,\mu_1{}^2 + 2187\,\mu_1\mu_3{}^3 = 0. \quad (2.75)$$

One should also consider the possibility of global bifurcations such as saddle to saddle connections off and on the free surface critical points. This requires ψ to attain the same value on and off the free surface critical points. The conditions for global bifurcation are

$$\left.\frac{\partial\psi}{\partial y}\right|_{y^2=-3\,\frac{x^2}{\omega}-\frac{\mu_2}{\omega}} = \mu_1 - 2\,\mu_2 x - 9\,\frac{\mu_3 x^2}{\omega} - 3\,\frac{\mu_3\mu_2}{\omega} - 8\,x^3 = 0,$$

$$\psi|_{y^2=-3\,\frac{x^2}{\omega}-\frac{\mu_2}{\omega}} = \mu_1 - 3\,\frac{\mu_3 x^2}{\omega} - \frac{\mu_3\mu_2}{\omega} - 2\,x^3 = 0, \quad (2.76)$$

and combining these gives

$$\begin{aligned}(4\,\mu_2{}^3 + 27\,\mu_1{}^2)(\omega^3\mu_1 - \mu_3{}^3 - \mu_2\mu_3\omega^2)(32\,\mu_2{}^6\omega^6 + 432\,\mu_2{}^4\mu_1\mu_3\omega^5 \\ + 1458\,\mu_2{}^2\mu_1{}^2\mu_3{}^2\omega^4 + 729\,\omega^3\mu_3{}^3\mu_1{}^3 + 540\,\omega^3\mu_2{}^3\mu_1\mu_3{}^3 + 2187\,\omega^2\mu_2\mu_1{}^2\mu_3{}^4 \\ - 108\,\omega^2\mu_2{}^4\mu_3{}^4 + 729\,\mu_1{}^2\mu_3{}^6 - 108\,\mu_2{}^3\mu_3{}^6) = 0. \quad (2.77)\end{aligned}$$

To analyse flow patterns in three parameters is rather academic. Therefore, we reduce the parameter number by using the following parameterization

$$\mu_2 = k\left(\frac{\mu_1}{2}\right)^{2/3} \quad \text{and} \quad \mu_3 = l\left(\frac{\mu_1}{2}\right)^{1/3}. \quad (2.78)$$

We find that bifurcation sets for $\mu_1 \neq 0$ become $k = -3$ and

$$64\,k^3\omega^4 + 1863\,k^2\omega^2 l^2 + 2187\,kl^4 - 3888\,lk\omega^3 + 1728\,\omega^4 - 1458\,\omega\,l^3 = 0, \quad (2.79)$$

and the global bifurcation occurs for

$$\begin{aligned}(k+3)(k^2 - 3\,k + 9)(2\,\omega^3 - l^3 - l\omega^2 k)(8\,\omega^6 k^6 + 216\,k^4 l\omega^5 - 27\,k^4 l^4\omega^2 \\ + 270\,k^3 l^3\omega^3 - 27\,k^3 l^6 + 1458\,l^2\omega^4 k^2 + 2187\,kl^4\omega^2 + 1458\,l^3\omega^3 + 729\,l^6) = 0 \quad (2.80)\end{aligned}$$

The reader will note that the bifurcation set on the free surface is almost the same as the bifurcation set of Bakker [1] and Gurcan *et al.* [12]. Although in this study the non-simple degenerate critical points are on the free surface, the flow patterns and their bifurcations are exactly the same as in Bakker [1] and Gurcan *et al.* [12] for $\omega = 1$, but the fixed wall is replaced by a free surface. The relevant computations are omitted and the bifurcation diagram is illustrated in Figure 6. It shows a degenerate flow pattern in which a separation bubble and a separating streamline interact with an in-flow saddle point creating two separation bubbles around flow centres with opposite rotations. This pattern is numerically observed in a double-film-fed forward roll coater. The bifurcation diagram for the normal form (2.69) with $\omega = -1$ is also shown in Figure 7.

https://doi.org/10.1017/S0956792512000319 Published online by Cambridge University Press

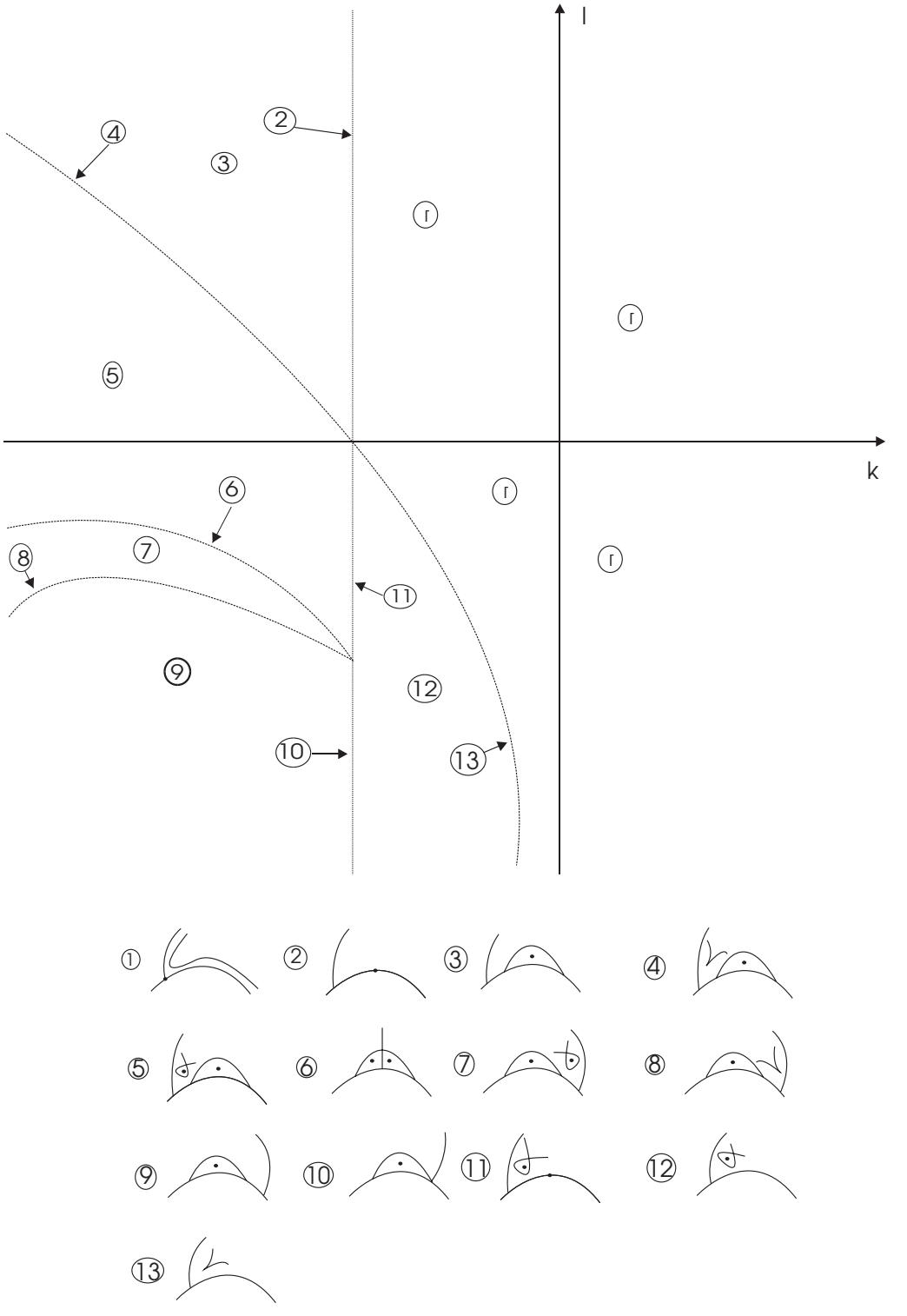

FIGURE 6. Bifurcation diagram for the normal form (2.69) with $\omega = 1$.

https://doi.org/10.1017/S0956792512000319 Published online by Cambridge University Press

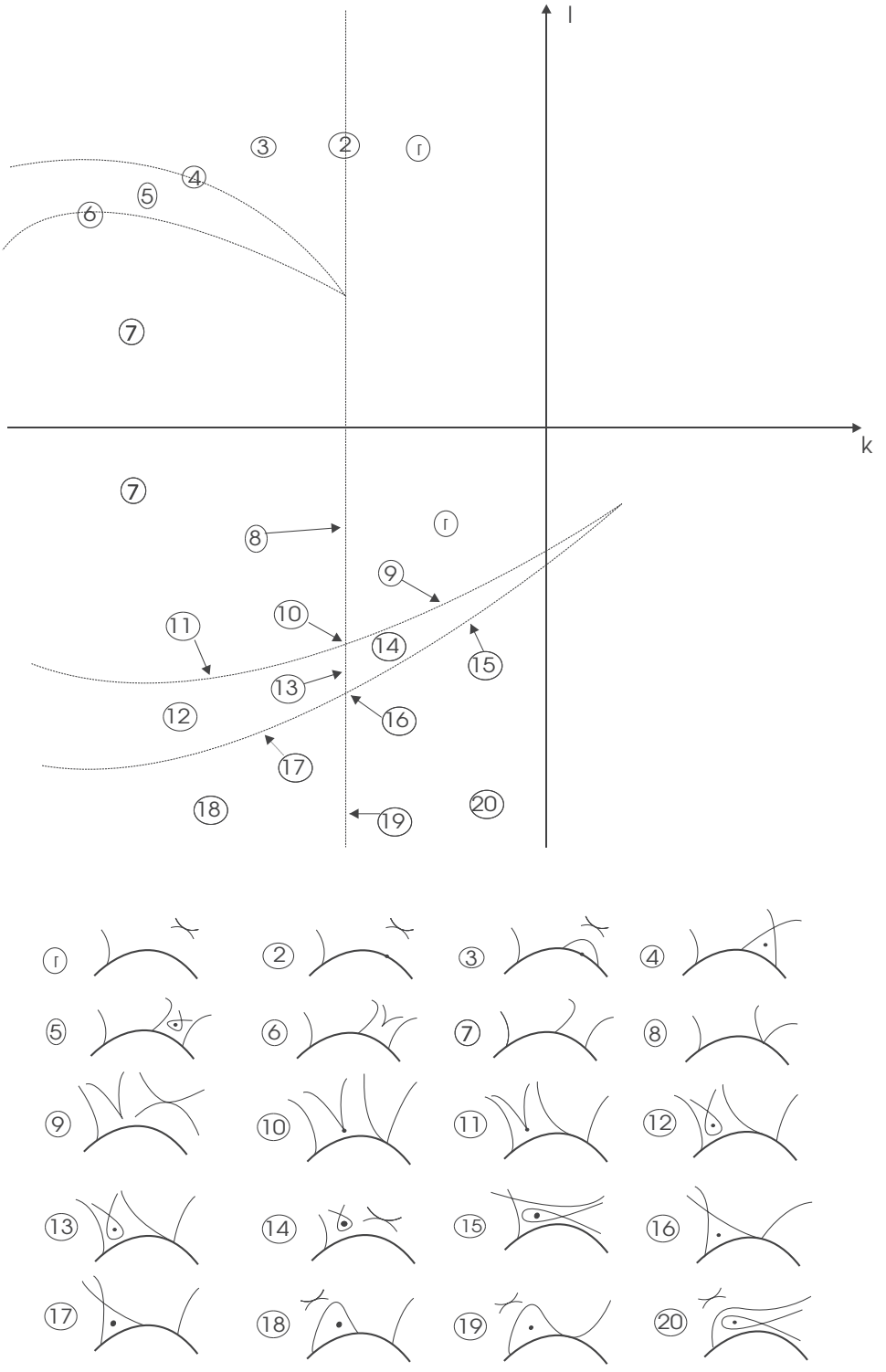

FIGURE 7. Bifurcation diagram for the normal form (2.69) with $\omega = -1$.

https://doi.org/10.1017/S0956792512000319 Published online by Cambridge University Press

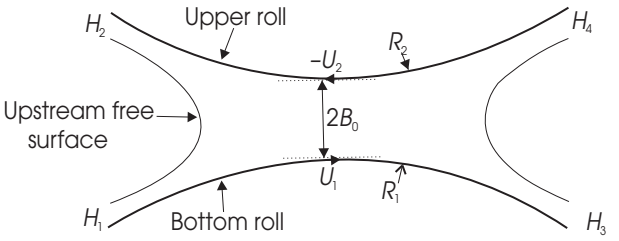

FIGURE 8. The reverse double-film-fed roll coating nip, see Wilson ([20], Figure 5.3).

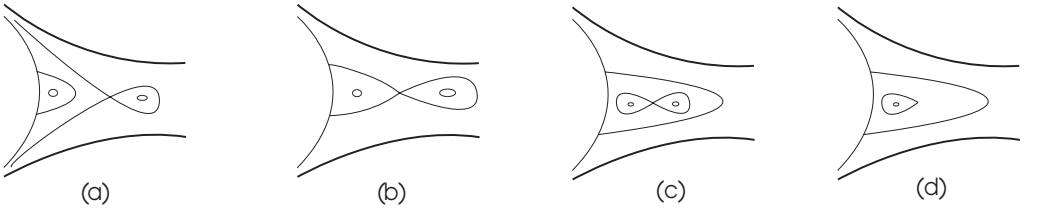

FIGURE 9. Schematic representation of flow patterns found by Wilson [20] in a reverse double-film-fed roll coating nip. Only the left of the nip is shown.

3 Application

Now we give a brief description of flow patterns found in a roll coater. A more description can be found in Wilson [20] and Wilson *et al.* [21]. Wilson [20] explored the development of flow structures in a reverse double-film-fed roll coater (reproduced in Figure 8). It illustrates the problem in which the rolls of radius R_1 and R_2 move in the opposite direction through the nip with peripheral speeds U_1 and $-U_2$ respectively. The surfaces of the rolls are separated by a minimum distance, $2B_0$, where B_0 is the semi-gap width. There is a gap between a pair of co-rotating rolls featuring four liquid films, $H[1], \ldots, H[4]$. The variation of the inlet film thickness is very important because it indicates the lubricant quantity that is being carried into the roll coater. Films H_1 and H_4/H_2 and H_3 are taken to be the incoming/outgoing films of thickness in the reverse double-film-fed roll coater. The resulting boundary value problem is described by five dimensionless parameters: the roll speed ratio $S = -U_2/U_1$; the returning film fraction $\zeta = H_4/H_2$; the inlet flux λ; the capillary number Ca and the radius to semi-gap ratio B_0/R.

In Figure 9 a series of flow structures is displayed for different values of the returning film fraction $\zeta = H_4/H_2$ at $Ca = 0.04$, $S = 1$, $B_0/R = 0.01$ and $\lambda = 0.3$. By variation of the returning film fraction, the flow patterns (a)–(d) in Figure 5 were obtained by Wilson ([20], Figures 5.31(d–f) and 5.35). In Figure 9(a), there exists a separation bubble on the upstream free surface and a homoclinic orbit at $\zeta = 0.78$. By decreasing ζ to around 0.243, the homoclinic orbit and the upstream separation bubble coalesce, thus connecting the interior saddle point to the two saddle points upstream the free surface, as seen in Figure 9(b). By decreasing ζ below 0.243, this global bifurcation results in one large upstream free surface with an inner separatrix which contains a saddle point and

https://doi.org/10.1017/S0956792512000319 Published online by Cambridge University Press

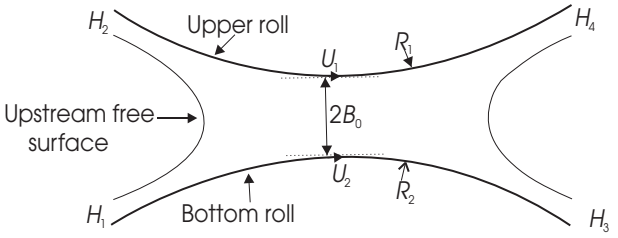

FIGURE 10. The forward double-film-fed roll coating nip, Wilson *et al.* ([21], Figure 2).

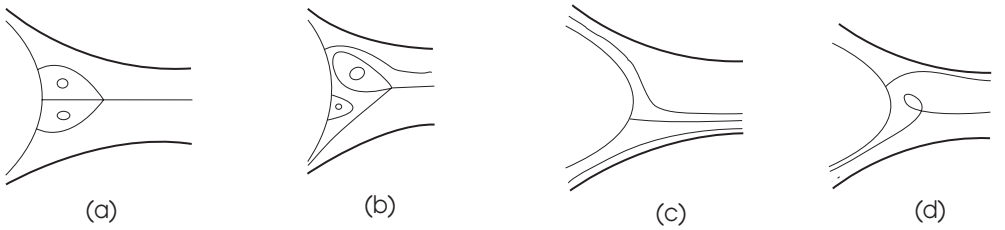

FIGURE 11. Schematics showing streamline patterns obtained by Wilson *et al.* [21] in a forward double-film-fed roll coating nip.

two sub-eddies (see Figure 9(c)). If the inlet flux λ was reduced, the downstream free surface would move upstream and the bead would shrink. Thus, the centre and the saddle would coalesce in a cusp bifurcation to leave just the centre on the left of the nip (see Figure 9(d)).

Wilson *et al.* [21] studied the steady flow in a double-film-fed forward roll coater (reproduced in Figure 10). As can be seen in Figure 10, the only difference between this problem and that in a reverse double-film-fed roll coater is the direction in which the upper roll moves. The dimensionless variables are given by the roll speed ratio $S = U_1/U_2$; the returning film fraction $\zeta = H_2/H_4$; the inlet flux λ; the capillary number Ca and the radius to semi-gap ratio B_0/R.

Flow patterns (a)–(d) shown in Figure 11 were found by Wilson *et al.* [21] (Figure 4(c), 8, 11(c) and (e) respectively). He first considered $S = 1$ and $\lambda = 0.21$ for decreasing ζ from 1 to 0.9. In particular, Figure 11(a) shows three saddle points on the free surface which interact with an in-flow saddle point creating two vortices with opposite rotations. As ζ is decreased, the heteroclinic connections separate from the saddle point on the free surface (see Figure 11(b)). Between each separation bubble and the separating streamline there is a homoclinic pattern. By varying the returning parameter ζ for other fixed parameters in Figures 11(c–d) one encounters the flow patterns and their bifurcations shown in Figure 6. The flow patterns 1, 5–6 and 12 in Figure 6 exactly correspond to patterns (a)–(d) in Figure 11. Wilson *et al.* [21] also stated that the flow pattern 7 in Figure 6 can be seen when $S < 1$, i.e. a homoclinic flow structure arises in the lower recirculation. The other flow patterns can be obtained at a slightly different values of ζ and λ, but with specific values of S. Therefore, a complete bifurcation diagram corresponding to Figure 6 is expected by varying the three physical parameters S, ζ and λ.

https://doi.org/10.1017/S0956792512000319 Published online by Cambridge University Press

4 Conclusion

In the present paper, the behaviour of degenerate flow patterns and their bifurcations near non-simple degenerate critical points on the free surface were considered by using the framework of local expansions of the stream function. We extend the classification of possible local streamline topologies close to a free surface by considering the fourth order expansion of the stream function in transformed coordinates. A simple stream function family was obtained using a normal form transformation and a variety of features, such as normal velocity, the tangential (shear) stress and normal stress condition, and the flow patterns were discussed. The flow patterns and bifurcations near a simple degenerate critical point were already studied by Brøns [3]. The present paper focused on 2D flow structures observed near a non-simple degenerate critical point on the free surface. These flow structures are of particular interest as they provide guidelines for complicated 3D flow structures. The possibilities are that the critical points in 3D flow structures are much greater than in 2D flow structures. Critical points for 2D flows can be of two types, either saddle or centre, but nodes and foci also exist as critical points in 3D flows. Also, global bifurcations cannot be determined by using a scalar stream function, since it does not exist for 3D flows. These suggest very complex dynamics and chaotic streamlines which the normal form cannot capture.

We obtain new flow patterns in Figure 4, such as an interaction of two vortices with opposite rotation as shown in Figure 4(c) that occur only near the non-simple degenerate critical point. The bifurcation diagram (Figure 5) is also obtained by Deliceoğlu and Gürcan [8] under the symmetric condition about a straight line away from boundaries in 2D incompressible flow. It was shown in [8] that the degenerate flow pattern (Figure 2(e)) does not occur in the steady flow with the mirror symmetry. Hence, the mechanisms of flow structures as shown in Figure 9 are not expected in the steady flow with the mirror symmetry. Furthermore, the bifurcation diagram (Figure 6) for the normal form (2.69) with $\omega = 1$, which was found near the wall by Bakker [1] and Gurcan *et al.* [12], is also seen close to the free surface by using different normal forms. We find no qualitative difference between flow topology in the rigid wall and the free surface. However, the degenerate flow pattern for $\omega = -1$ in Figure 3 and their bifurcations as shown in Figure 7 have not been previously observed close to rigid wall or any boundaries.

The theory was applied to the pattern found numerically in the studies of Stokes flow in the double-film-fed reverse and forward roll coater. The application of the theory was already carried out by Wilson *et al.* [21] for Stokes flow in the bead of a meniscus roll coater. Gurcan *et al.* [12] also observed similar transformation of flow patterns in a double-lid-driven cavity except that the pattern (12) in Figure 6 cannot appear in the cavity for the considered values of (S, A) parameters, i.e. the flow configuration jumps from type (9) to type (13) in Figure 6.

Acknowledgement

The author wishes to thank Prof. Dr. F. Gürcan and Dr. M. Wilson for their valuable support, comments, suggestions and corrections.

References

[1] Bakker, P. G. (1991) *Bifurcation in Flow Patterns, Vol. 2: Nonlinear Topics in the Mathematical Sciences*, Klüver, Dordrecht, Netherlands.

[2] Bisgaard, A. V., Brøns, M. & Sørensen, J. N. (2006) Vortex breakdown generated by off-axis bifurcation in circular cylinder with rotating covers. *Acta Mech.* **187**, 75–83.

[3] Brøns, M. (1994) Topological fluid dynamics of interfacial flows. *Phys. Fluids* **6**, 2730–2736.

[4] Brøns, M. & Bisgaard, A. V. (2006) Bifurcation of vortex breakdown patterns in a circular cylinder with two rotating covers. *J. Fluid Mech.* **568**, 329–349.

[5] Brøns, M. & Hartnack J. N. (1999) Streamline topologies near simple degenerate critical points in two-dimensional flow away from boundaries. *Phys. Fluids* **11**, 314–324.

[6] Brøns, M., Jakobsen B., Niss, K., Bisgaard, A. V. & Voigt, L. K. (2007) Streamline topology in the near-wake of a circular cylinder at low Reynolds numbers. *J. Fluid Mech.* **584**, 23–43.

[7] Brøns, M., Voigt, L. K. & Sørensen J. N. (2001) Topology of vortex breakdown bubbles in a cylinder with a rotating bottom and a free surface. *J. Fluid Mech.* **428**, 133–148.

[8] Deliceoğlu, A. & Gürcan, F. (2008) Streamline topologies near non-simple degenerate critical points in two-dimensional flow with symmetry about an axis. *J. Fluid Mech.* **606**, 417–432.

[9] Golubitsky, M. & Guillemin, V. (1973) *Stable Mappings and Their Singularities*, Springer-Verlag, New York.

[10] Gostling, M. J., Savage, M. D. & Wilson, M. C. T. (2001) Flow in a double-film-fed fluid bead between contra-rotating rolls. II. Bead break and flooding. *Euro. J. Appl. Math.* **12**, 413–431.

[11] Gürcan, F. & Deliceoğlu, A. (2005) Streamline topologies near non-simple degenerate points in two-dimensional flows with double symmetry away from boundaries and an application. *Phys. Fluids* **17**, 093106(1–7).

[12] Gürcan, F., Deliceoğlu, A. & Bakker, P. G. (2005) Streamline topologies near non-simple degenerate point close to a stationary wall using normal forms. *J. Fluid Mech.* **539**, 299–311.

[13] Hartnack, J. N. (1999) Streamlines topologies near a fixed wall using normal forms. *Acta Mech.* **136**, 55–75.

[14] Lugt, H. J. (1987) Local flow properties at a viscous free surface. *Phys. Fluids* **30**, 3647–3652.

[15] Mather, J. N. (1977) Differentiable invariants. *Topology* **16**, 145–155.

[16] Moser, J. (1973) *Stable and Random Motions in Dynamical Systems,* Princeton University Press, Princeton, NJ.

[17] Summers, J. L., Thompson, H. M. & Gaskell, P. H. (2001) Flow structure and transfer jets in a contra-rotating rigid-roll coating system. *Theoret. Comput. Fluid Dyn.* **17**, 189–212.

[18] Thom, R. (1975) *Structural Stability and Morphogenesis*, W. A. Benjamin, Reading, MA (original edition, Paris, 1972).

[19] Tophøj, L., Møller, S. & Brøns, M. (2006) Streamline patterns and their bifurcations near a wall with Navier slip boundary conditions. *Phys. Fluids* **18**, 083102.

[20] Wilson, M. C. T. (1997) *Free Surface Flows Between Co-Rotating and Contra-Rotating Cylinders*, PhD thesis, University of Leeds, Leeds, UK.

[21] Wilson, M. C. T., Gaskell, P. H. & Savage, M. D. (2001) Flow in a double-film-fed fluid bead between contra-rotating rolls. I. Equilibrium flow structure. *Euro. J. Appl. Math.* **12**, 395–411.